The role of cascade energy and temperature in primary defect formation in iron

Roger E. Stoller*

Metals and Ceramics Division, Oak Ridge National Laboratory, P.O. Box 2008, Oak Ridge, TN 37831-6376, USA

Abstract

Molecular dynamics (MD) simulations have been used to investigate the formation of atomic displacement cascades in iron with energies up to 50 keV (corresponding to a primary knock-on atom (PKA) energy of 79 keV) at 100 K, up to 20 keV at 600 K, and up to 10 keV at 900 K. The cascade damage production has been characterized in terms of several parameters: the number of surviving point defects, the fraction and type of surviving point defects found in clusters, and the size distributions of the in-cascade point defect clusters. A sufficient number of simulations have been completed at each condition to evaluate the statistical variation in these primary damage parameters as a function of irradiation temperature and cascade energy. The energy dependence of stable defect formation can be conveniently separated into three regimes with the number of defects in each regime correlated by a simple power law with a characteristic exponent. The primary effects of cascade energy on defect formation at high energies are explained in terms of subcascade formation. Only a modest effect of temperature is observed on defect survival, while irradiation temperature increases lead to a slight increase in the in-cascade interstitial clustering fraction and a decrease in the vacancy clustering fraction. Cascade energy has little effect on the in-cascade clustering fractions above about 5 keV. However, there is a systematic change in the cluster size distribution, with higher energy cascades producing larger clusters. The loosely coupled nature of the in-cascade vacancy clusters persists at higher energies. © 2000 Elsevier Science B.V. All rights reserved.

1. Introduction

The method of molecular dynamics (MD) has been broadly applied in recent years to the investigation of primary damage formation in irradiated materials [1–10]. Modern, high speed computers with large amounts of memory have permitted researchers to examine higher energy events with their requirement for larger numbers of atoms. These same computing resources have permitted cascade simulations to be completed in sufficient numbers to obtain statistically meaningful mean values, and for comparisons to be made between different materials. For example, a previously reported comparison of cascade damage formation in iron and copper was based on a database of over 600 cascades [5]. The results presented in that study comprise cascade energies from 60 eV to 10 keV for irradiation temperatures of 100 and 600 K, and up to 5 keV at 900 K. The average number of

defects that survived in the iron and copper MD cascade simulations at each energy was also compared with the number of displacements obtained from the standard secondary displacement model by Norgett, Robinson, and Torrens (NRT) [11] with the recommended value of the atomic displacement threshold for both materials [12].

MD investigations of displacement cascades in a number of materials have established several consistent trends in primary damage formation. These trends include: (1) the total number of stable point defects produced follows a power-law dependence on the cascade energy over a broad energy range, (2) the ratio of MD stable displacements divided by the number obtained from the NRT model decreases with energy until subcascade formation becomes prominent, (3) the in-cascade clustering fraction of the surviving defects increases with cascade energy, and (4) the effect of lattice temperature on the MD results is rather weak. Two additional observations have been made regarding in-cascade clustering in iron. First, the interstitial clusters have a complex, three-dimensional morphology, with

_____

* Tel.: +1-423 576 788; fax: +1-423 574 0641.

E-mail address: rkn@ornl.gov (R.E. Stoller).

both sessile and glissile configurations. Mobile interstitial clusters appear to glide with a low activation energy similar to that of the mono-interstitial (∼0.1–0.2 eV) [13]. Second, the vacancy clustering fraction is much lower than the interstitial clustering fraction. If based on a nearest-neighbor clustering criterion, the fraction of surviving vacancies and interstitials in clusters for high energy cascades is about 3% and 20% of the NRT displacements, respectively.

The results presented here summarize further statistical analysis of the iron cascade database completed at lower energies to provide a more complete characterization of the energy and temperature dependence of cascade damage production. Additional cascade simulations have extended the range of the previous studies to a peak cascade energy of 50 keV at 100 K and 20 keV at 600 K. Completing higher energy simulations provides an opportunity to validate the trends established at lower energies. In particular, they further probe the energy domain of extensive subcascade formation. Both the total number of point defects produced and the fraction of these defects found in clusters at the end of the cascade event appeared to be relatively independent of temperature at the lower energies. The in-cascade cluster size distributions exhibit more temperature dependence at the higher energies, with vacancy clustering decreasing and interstitial clustering increasing as the temperature increases.

2. MD simulation method

The calculations were carried out using the MOLDY [14] MD code and the interatomic potential for iron developed by Finnis and Sinclair for α-iron [15,16] and subsequently modified by Calder and Bacon [3]. This code and potential have been widely used, and are discussed in detail elsewhere [2–10]. The simulations were carried out using periodic boundary conditions and at constant pressure. Since the boundary atoms were not damped to remove heat, the initiation of a cascade event led to some lattice heating. The primary impact of the temperature increase is to extend the lifetime of the thermal spike, it has little or no impact on the ballistic phase of the cascade. The effect of this temperature increase on primary damage formation is not yet clear. There is some evidence that the adiabatic conditions may have an impact on the in-cascade interstitial clustering fraction [17]. In addition, although previous work has not shown a significant impact of temperature on total defect survival [3,5,10], some of the results presented here suggest that relatively large temperature increases may reduce the number of stable point defects produced.

Prior to conducting the cascade simulations, a block of atoms was thermally equilibrated at the temperature of interest for about 10 ps. This equilibrated atom block was used as the starting point for the subsequent cascade simulations; the size of the block is increased for higher energy simulations as shown in Table 1. The simulations were initiated by giving a lattice atom the specified amount of kinetic energy and an initial direction; a high index lattice direction such as ⟨135⟩ was typically used to minimize channeling. Additional cascades were differentiated by changing the location of the primary knock-on atom (PKA) or by using a different equilibrated atom block. As discussed in Ref. [5], the initial kinetic energy is analogous to the damage energy in the NRT [11] model. The kinetic energy lost to electronic excitation accounts for the difference between the PKA energy and damage energy and this energy loss mechanism is not simulated in the MOLDY code [5]. Both the MD simulation energies and the corresponding PKA energies are listed in Table 1. The neutron energies listed in Table 1 are those for which the PKA energy is the average recoil energy in an elastic collision. Note that these MD simulations account for recoils from neutrons that are well into the high (fast) energy domain, i.e. energies greater than about 0.1 MeV.

Table 1
Typical particle energy parameters, corresponding NRT displacements, and simulation cell size for MD cascade simulations

Neutron energy (MeV)	Average PKA energy (keV)	Corresponding E_{MD} (keV)	NRT displacements	Atoms in simulation
0.0034	0.116	0.1	1	3456
0.0058	0.236	0.2	2	6750
0.014	0.605	0.5	5	6750
0.036	1.24	1	10	54 000
0.074	2.54	2	20	54 000
0.19	6.60	5	50	128 000
0.40	13.7	10	100	250 000
0.83	28.8	20	200	250 000
1.8	61.3	40	200	1 024 000
2.3	78.7	50	500	2 249 728

3. Primary damage formation in MD simulations

The parameters used in the following discussion to describe results of MD cascade simulations are the total number of surviving point defects and the fraction of the surviving defects contained in clusters. The number of surviving defects will be expressed as a fraction of the NRT displacements listed in Table 1, whereas the number of defects in clusters will be expressed as either a fraction of the NRT displacements or a fraction of the total surviving MD defects. The criterion used to define a point defect cluster in this study was that each defect in the cluster must be in a nearest-neighbor position to another defect. As discussed below, defect clusters are not necessarily compact structures under this definition. In order to analyze the statistical variation in the primary damage parameters, the mean value (M), the standard deviation about the mean (σ), and the standard error of the mean (ε) have been calculated for each set of cascades conducted at a given energy and temperature. The standard error of the mean is calculated as $\varepsilon = \sigma/n^{0.5}$, where n is the number of cascade simulations

completed [18]. The standard error of the mean provides a measure of how well the sample mean represents the actual mean. For example, a 90% confidence limit on the mean is obtained from $1.86 * \varepsilon$ for a sample size of nine [19]. These statistical quantities are summarized in Table 2 for total defect survival and interstitial clustering. Work is in progress to obtain a more complete temperature comparison, e.g. 10 keV cascades at 600 K and 20 keV cascades at 900 K.

3.1. Total point defect survival

Previous work indicates that the number of stable displacements (vacancy–interstitial pair) remaining at the end of a cascade simulation, N_D, exhibits a power-law dependence on cascade energy [7,8]. For example, after analyzing simulations in iron between 0.5 and 10 keV at 100 K, Bacon et al. found that the total number of surviving point defects could be expressed as [7]

$$N_D = 5.67 E_{MD}^{0.779}, \tag{1}$$

Table 2
Statistics of primary damage parameters derived from MD cascade simulations

Temperature (K)	Energy (keV)	Number of cascades	Surviving displacements (mean/ standard deviation/standard error)		Clustered interstitials (mean/standard deviation/standard error)		
			Number	Per NRT defects	Number	Per NRT defects	Per MD surviving defects
100	5	8	17.1	0.343	8.38	0.168	0.488
			2.59	0.0517	1.85	0.0369	0.0739
			0.916	0.0183	0.654	0.0130	0.0261
	10	15	33.6	0.336	17.0	0.170	0.506
			5.29	0.0529	4.02	0.0402	0.101
			1.37	0.0137	1.04	0.0104	0.0261
	20	10	60.2	0.301	36.7	0.184	0.610
			8.73	0.0437	6.50	0.0325	0.0630
			2.76	0.0138	2.06	0.0103	0.0199
	30	9	93.2	0.311	n/c[a]	n/c	n/c
			14.9	0.0498			
			4.98	0.0166			
	40	8	131.0	0.328	74.5	0.186	0.570
			12.6	0.0315	15.0	0.0375	0.102
			4.45	0.0111	5.30	0.0133	0.0361
	50	9	168.3	0.337	93.6	0.187	0.557
			12.1	0.0242	6.95	0.0139	0.0432
			4.04	0.00807	2.32	0.00463	0.0144
600	20	8	55.8	0.279	41.6	0.208	0.747
			5.90	0.0295	5.85	0.0293	0.0782
			2.09	0.0104	2.07	0.0104	0.0276
900	10	7	27.3	0.273	18.6	0.186	0.677
			5.65	0.0565	6.05	0.0605	0.1605
			2.14	0.0214	2.29	0.0229	0.0607

[a] n/c denotes that the analysis of interstitial clusters is not completed at this time.

where the cascade energy, E_{MD} is given in keV. This relationship did not hold below about 0.5 keV because true cascade-like behavior does not occur at these low energies. Subsequent work by Stoller [8,10] indicated that N_D also begins to deviate from this energy dependence above 20 keV when extensive subcascade formation occurs. New results at 30 and 50 keV confirm that the energy dependence of defect survival changes near 20 keV. This is illustrated in Fig. 1(a), where Eq. (1) is plotted along with the average number of surviving interstitials at energies up to 50 keV. At each energy, the data point is an average of between 7 and 26 cascades. Error bars are included for the 10–50 keV data to indicate the standard error of the mean. The range of plus or minus one standard error is barely detectable around the data points, indicating that the change in slope is statistically significant.

In addition to the new results at 30 and 50 keV, two of the values in Fig. 1 are different from those reported previously [3,5,10]. As part of an investigation of the influence of pre-existing damage on defect formation, eight 10 keV simulations at 100 K were carried out in perfect crystal to provide the baseline for comparison. The results of these eight simulations have been averaged together with the seven reported previously. This resulted in a negligible change in the average number of surviving defects from 33.9 to 33.6. This small change in average is consistent with the small standard errors shown in Fig. 1. A more significant change has been made in the value at 0.3 keV. Although 16 cascade simulations were completed at this energy by Calder and Bacon [3], the total point defect survival and interstitial clustering fraction values obtained at 0.3 keV appeared to be inconsistent with the rest of the data. Ten additional simulations have been carried out and the new average of all 26 simulations is used in this paper. With this new data, it appears that three well-defined regions

with different energy dependencies exist. A power-law fit to the points in each energy region is shown in Fig. 1(a). The best-fit exponent in the absence of true cascade conditions below 0.5 keV is 0.485. From 0.5 to 20 keV, the exponent is 0.795. This is marginally higher than the value in Eq. (1), possibly because the 20 keV data were used in the current fitting. An exponent of 1.12 was found in the range above 20 keV which is dominated by subcascade formation. In each energy range, the MD results deviate from the linear energy dependence predicted by the NRT model.

The data from Fig. 1(a) are replotted in Fig. 1(b) where the number of surviving displacements is divided by the NRT displacements at each energy. The rapid decrease in this MD defect survival ratio at low energies is well known. The error bars again reflect the standard error and the solid line through the points is a least-squares fit to the energy dependence that was used in an assessment of neutron energy spectrum effects [20]. Note that at very low energies, the number of surviving displacements in the MD simulations exceeds the NRT value. This is a result of using the average displacement threshold energy of 40 eV in the NRT model. The actual displacement threshold varies with crystallographic direction and is as low as ~19 eV in the [1 0 0] direction [21]. This simply implies that the low energy (near threshold) simulations preferentially produce displacements in the 'easy' directions [22].

Just as the 30–50 keV data points fall above the values predicted by the mid-energy power-law curve in Fig. 1(a), the surviving defect fraction shows a slight increase as the cascade energy increases from 20 to 50 keV, and the standard errors shown indicate that the increase is statistically significant. Although it is not possible to quantitatively associate a specific defect survival fraction with a given cascade morphology, it is interesting to compare 10 and 50 keV cascades since the
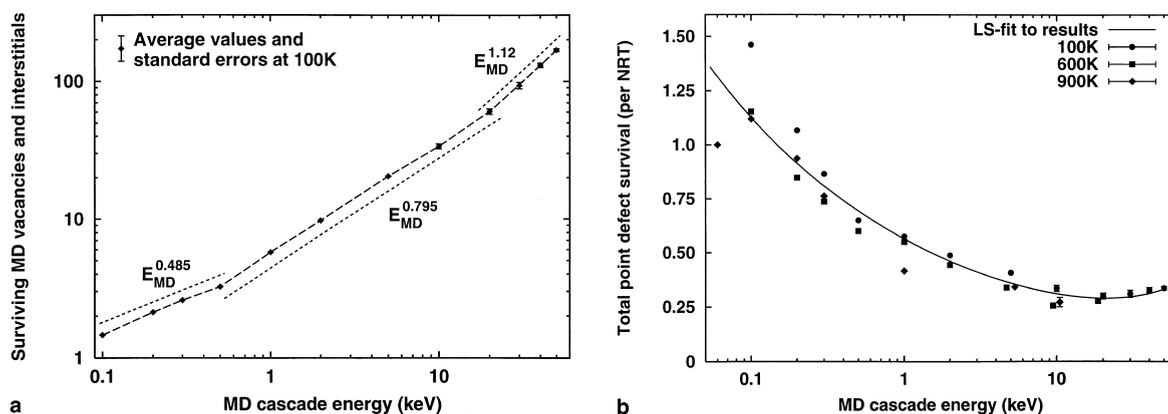

Fig. 1. Cascade energy dependence of stable point defect formation in iron MD cascade simulations: (a) total number of interstitials or vacancies at 100 K; (b) ratio of defects to NRT displacements. Data points indicate mean values at each energy and error bars indicate standard error of the mean.

defect survival fractions are nearly the same at both energies. Such a comparison is shown in Fig. 2, where the peak damage state from typical 10 and 50 keV cascades are displayed. An average defect survival fraction of ~0.3 as shown for the 10–50 keV cascades is consistent with values estimated from resistivity change measurements following low-temperature neutron irradiation [22,23].

Although it is difficult to discern a consistent effect of temperature between the 600 and 900 K data points, the defect survival fraction at 100 K is always somewhat greater than at either of the two higher temperatures. This is in agreement with the effect of temperature reported by Gao et al. [17] in their study of 2 and 5 keV cascades. Calculated mean survival values and standard errors for 10 keV cascades at 900 K, and 20 keV cascades at 600 K are shown in Fig. 1(b). These results also indicate a significant reduction in defect survival with increasing temperature. Further verification of the temperature dependence of defect survival will be provided by work which is currently in progress: a statistical analysis of all the lower energy cascades, and the completion of 10 and 20 keV cascades simulations at 600 and 900 K, respectively.

3.2. In-cascade interstitial clustering

The dependence of in-cascade interstitial clustering on cascade energy is shown in Fig. 3 for simulation temperatures of 100, 600, and 900 K, where the average number of interstitials in clusters has been divided by the corresponding number of NRT displacements. Statistical parameters are listed in Table 2 and the number of cascades is the same as in Fig. 1. The solid line in Fig. 3(a) is again the least-squares fit to the data that was
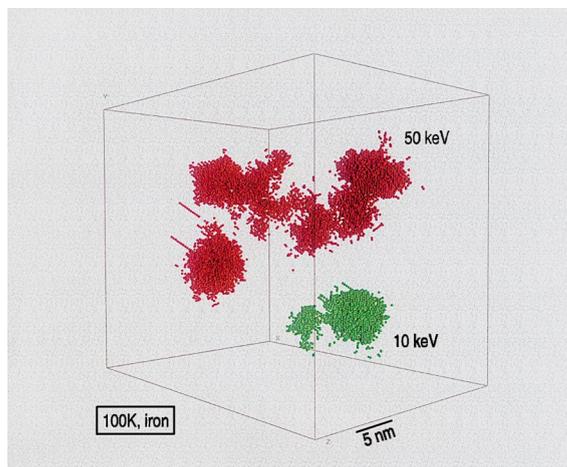

Fig. 2. Illustration of typical cascade morphology and subcascade formation in 10 and 50 keV simulations.

used to help assess neutron energy spectrum effects [20]. Data points at 0.1, 10, and 20 keV have been slightly offset along the energy axis to help visually distinguish between the results. Although no physical significance should be assigned to the structure of the curve above 10 keV in Fig. 3(a), it can be understood by considering Figs. 1(b) and 3(b). The clustering per NRT (Fig. 3(a)) is essentially the product of clustering per MD (Fig. 3(b)) times the surviving MD defects per NRT (Fig. 1(b)).

Considerable scatter is observed in the clustering fraction at low energies. This may be partially a result of differences between the tools used to characterize the low and high energy cascades. The higher energy simulations required more sophisticated visualization tools, and this potential difference has prompted the reanalysis of the lower energy cascades which is now in progress. Overall, the interstitial clustering fraction exhibits more variability between cascades at the same energy than does defect survival, and the validity of the indicated fit is therefore less certain. The standard errors in Fig. 3(a) are much larger than the corresponding values for the defect survival fraction. The fraction of interstitials in clusters is zero at the lowest energies and appears to saturate at about 18–20% of the NRT displacements above 5 keV, which corresponds to about 60% of the total surviving interstitials. Although it is not possible to discern a systematic effect of temperature below 10 keV, there is an apparent trend toward greater clustering with increasing temperature at higher energies. This can be more clearly seen in Fig. 3(b), where the ratio of clustered interstitials to surviving interstitials is shown, and in the cluster size distributions that will be discussed below. Such an effect of temperature on interstitial clustering in these adiabatic simulations is consistent with that observed by Gao et al. [17] in their work with a hybrid MD model that extracted heat from the simulation cell, i.e. the found that the clustering fraction increases with temperature.

The interstitial cluster size distributions exhibit a consistent dependence on cascade energy and temperature as shown in Fig. 4 (where a size of 1 denotes the single interstitial). The cascade energy dependence at 100 K is shown in Fig. 4(a), where only the size distributions at 10 and 50 keV are included to simplify the figure. The influence of cascade temperature is shown for 10 keV cascades in Fig. 4(b), and for 20 keV cascades in Fig. 4(c). All interstitial clusters larger than size 10 are combined into a single class in the histograms in Fig. 4. The interstitial cluster size distribution shifts to larger sizes as either the cascade energy or temperature increases. An increase in the clustering fraction at the higher temperatures is most clearly seen as a decrease in the number of mono-interstitials. Comparing Fig. 4(b) and (c) demonstrates that the temperature dependence increases as the cascade energy increases. The largest interstitial cluster observed in these simulations was
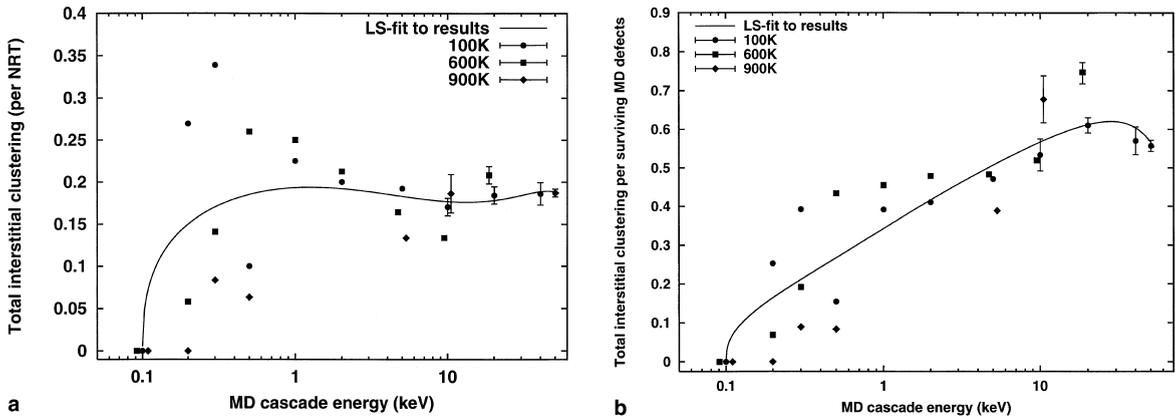
Fig. 3. Cascade energy dependence of interstitial clustering: (a) clustered interstitials divided by NRT displacements; (b) clustered interstitials divided by total surviving interstitials. Data points indicate mean values and error bars indicate standard error of the mean.
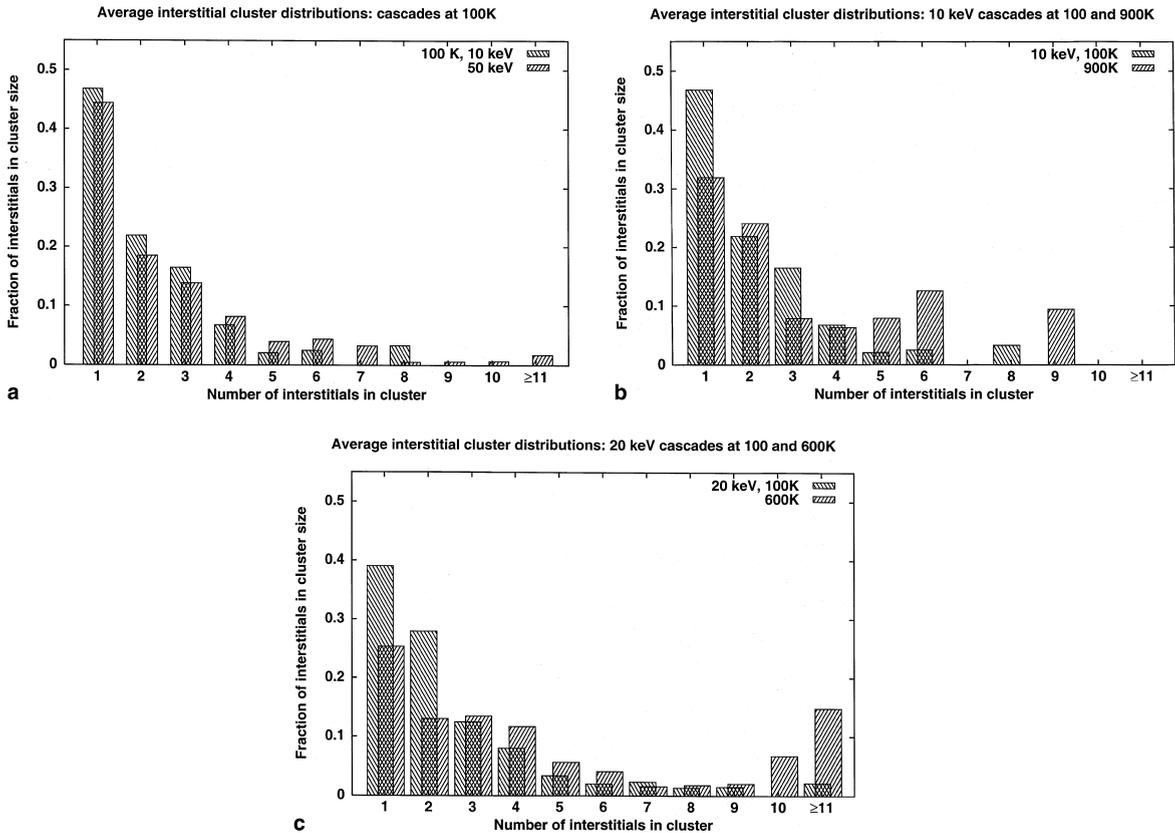

Fig. 4. Fractional size distributions of interstitial clusters formed directly within the cascade, comparison of: (a) 10 and 50 keV cascades at 100 K; (b) 10 keV cascades at 100 and 900 K; (c) 20 keV cascades at 100 and 600 K.

contained in a 20 keV cascade at 600 K as shown in Fig. 5. This large cluster was composed of 33 interstitials ($\langle 1\,1\,1 \rangle$ crowdions and dumbbells), and exhibited considerable mobility via what appeared to be one-dimensional glide in a $\langle 1\,1\,1 \rangle$ direction [10].

The increase in the number of large clusters at high energies and temperatures suggested that the in-cascade cluster size distributions may exhibit more sensitivity to neutron energy spectrum than did either total defect survival or the total interstitial clustering fraction. At
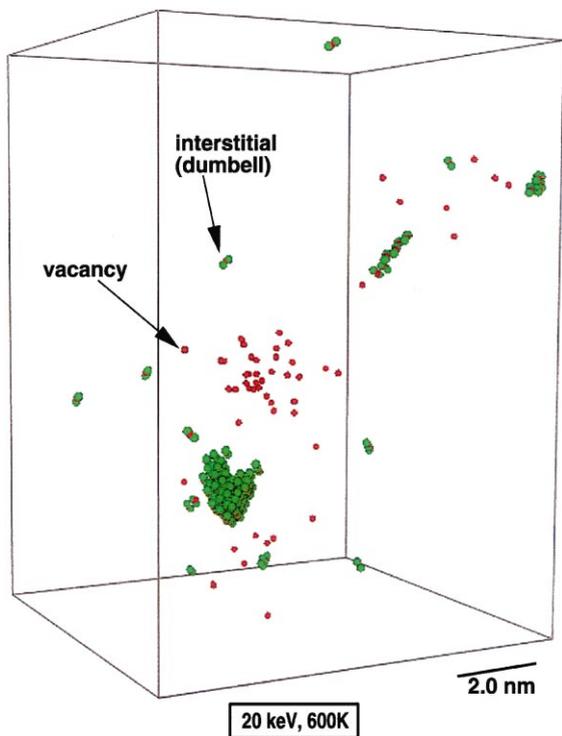
Fig. 5. Residual defects at ~30 ps from a 20 keV cascade at 100 K containing a 33-interstitial cluster.

uncommon, the fraction of interstitials contained in them is correspondingly small. This leads to the relatively large standard errors shown in the figure. The 33-interstitial cluster shown in Fig. 5 plays a significant role in the sharp increase in this clustering fraction observed between 100 and 600 K for the 20 keV cascades. A least-squares fit to the three 100 K results is shown by the solid line in Fig. 6. Although the statistical basis for using the curve in Fig. 6 is more limited than for the curves in Figs. 1(b) and 3, this partial clustering fraction was also included in the evaluation of neutron spectrum effects discussed in Ref. [20]. The average fraction of interstitials in large in-cascade clusters for several neutron irradiation environments was obtained by weighting the function shown in Fig. 6 with their respective PKA spectra. These spectrum-averaged clustering values exhibited a significant variation between the various

100 K, there are no interstitial clusters larger than 8 for cascade energies of 10 keV or less. Therefore, the fraction of interstitials in clusters of 10 or more was chosen as an initial parameter for evaluation of the size distributions. This partial interstitial clustering fraction is shown in Fig. 6. Since the large clusters are relatively
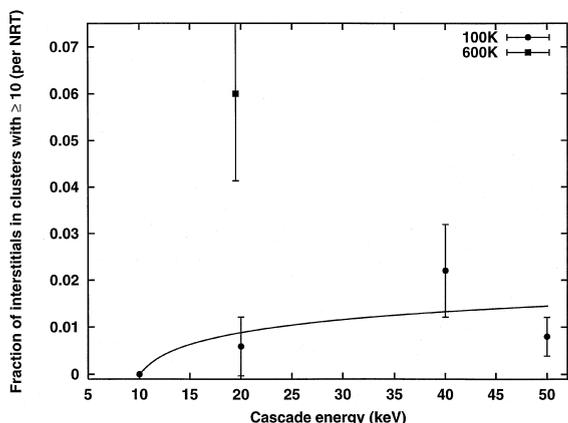
Fig. 6. Cascade energy dependence of interstitials contained in clusters of 10 or more: clustered interstitials divided by NRT displacements. Data points indicate mean values and error bars indicate standard error of the mean.
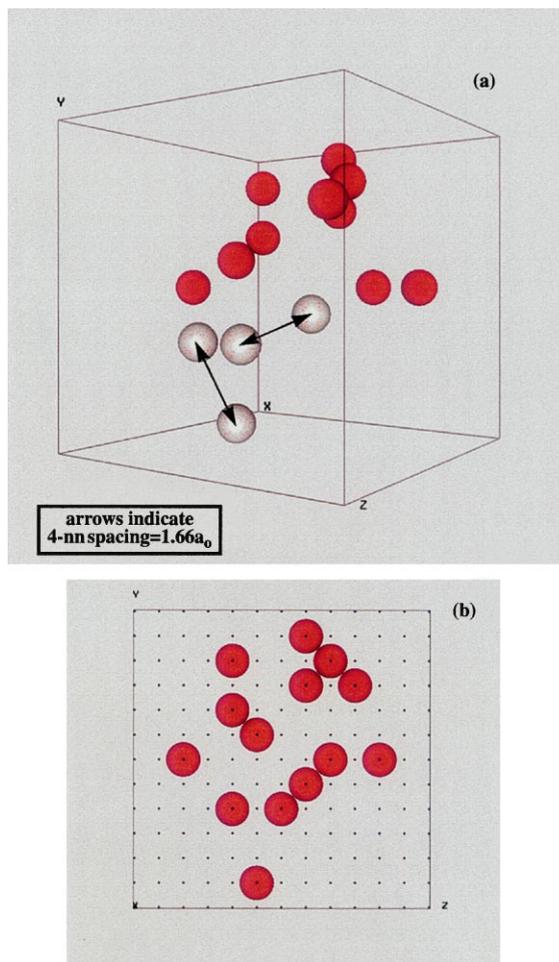

Fig. 7. Typical uncollapsed or nascent vacancy cluster from 50 keV cascade at 100 K; 14 vacancies are contained, each of which is within the 4-nn distance ($1.66a_o$). Perspective view shown in (a) and an orthographic projection in (b).

environments. This is in contrast to the spectrum-averaged total defect survival and total interstitial clustering fractions which show little dependence on neutron energy spectrum.

3.3. In-cascade vacancy clustering

As reported previously [5,10], the in-cascade vacancy clustering fraction in iron is quite low ($\sim$3% of NRT) when the nearest-neighbor (nn) criterion for clustering is applied. When an analysis of the spatial arrangement of the surviving vacancies in 10, 20, and 40 keV cascades was conducted, peaks in the distribution were obtained for vacancies in second (2-nn) and fourth (4-nn) nearest neighbor locations [10]. Similar results were obtained from the analysis of the vacancy distributions in 50 keV cascades at 100 K and the 20 keV cascades 600 K. The peak observed for vacancies in 2-nn locations is consistent with the di-vacancy binding energy being greater for 2-nn (0.22 eV) than for 1-nn (0.09 eV) [24]; the reason for the peak at 4-nn is unclear.

An example of these uncollapsed vacancy clusters is shown in Fig. 7 where a collection of 14 vacancies has been extracted from a 50 keV cascade at 100 K. Each of the vacancies has at least one other vacancy within the 4-nn spacing of $1.66a_o$. The 'cluster' is shown in two views; a 3-D perspective view is shown in Fig. 7(a), and an orthographic projection ($-x$) in Fig. 7(b). Such an arrangement of vacancies is similar to some of the vacancy clusters observed by Sato et al. in field ion microscope images of irradiated tungsten [25]. Since the time of the MD simulations is too short to allow vacancies to jump ($\leqslant$ 100 ps), the possibility that these closely correlated vacancies might collapse into clusters over somewhat longer times has been investigated using Monte Carlo (MC) simulations. The vacancy coordinates at the end of the MD simulations were extracted and used as the starting configuration in MC cascade annealing simulations. The expectation of vacancy clustering was confirmed in the MC simulations, where many of the isolated vacancies had clustered within 70 µs [24,26].

The energy and temperature dependence of in-cascade vacancy clustering as a fraction of the NRT displacements is shown in Fig. 8 for cascade energies of 10–50 keV. Results are shown for clustering criteria of 1-nn, 2-nn, 3-nn, and 4-nn. A comparison of Figs. 8 and 3 indicates that in-cascade vacancy clustering in iron remains lower than that of interstitials even when the 4-nn criterion is used. This is consistent with the experimentally observed difficulty of forming visible vacancy clusters in iron as discussed in Ref. [5], and the fact that only relatively small vacancy clusters are found in positron annihilation studies of irradiated ferritic alloys [27]. The cascade energy dependence of vacancy clustering is similar to that of interstitials; a slight increase in vacancy clustering is observed as the cascade energy
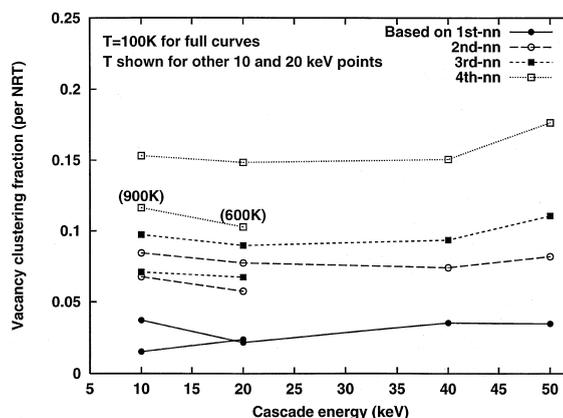

Fig. 8. Cascade energy dependence of vacancy clustering: clustered vacancies divided by NRT displacements. Data points indicate mean values and error bars indicate standard error of the mean.

increases from 10 to 50 keV. However, vacancy clustering decreases as the temperature increases.

Fractional vacancy cluster size distributions are shown in Fig. 9, for which the 4-nn clustering criterion has been used. Fig. 9(a) illustrates that the vacancy cluster size distribution shifts to larger sizes as the cascade energy increases from 10 to 50 keV. This is similar to the change shown for interstitial clusters in Fig. 4(a). There is a corresponding reduction in the fraction of single vacancies. However, as mentioned above, the effect of cascade temperature shown in Fig. 9(b) and (c) is opposite to that observed for interstitials. The magnitude of the temperature effect on the vacancy cluster size distributions also appears to be weaker than in the case of interstitial clusters. The fraction of single vacancies increases and the size distribution shifts to smaller sizes as the temperature increases from 100 to 900 K for the 10 keV cascades, and from 100 to 600 K for 20 keV cascades. As seen for interstitial clusters, the effect of temperature seems to be greater at 20 keV than at 10 keV.

4. Discussion and summary

As part of an ongoing effort to characterize primary damage formation in iron, MD displacement cascade simulations have been conducted at energies up to 50 keV and temperatures up to 900 K. A sufficient number of cascades have been completed to begin a statistical evaluation of the results. For example, the calculated standard errors of the mean values at any one energy are small enough to establish significant trends in the energy dependence. In the case of simulations at 100 K, three well-defined energy regimes are observed. The

total number of surviving defects in each of these regimes can be well fit with a simple power law. The lowest energy dependence, with an exponent of 0.485, is observed at energies below 0.5 keV, where well-developed cascades do not occur. This low energy exponent may arise from the discrete way in which displacements occur in events near the threshold. Once the first displacement is produced, a greater fraction of the damage energy is lost to lattice phonons, as opposed to atomic displacements, until sufficient energy is available to create the second or third displacement. The angular dependence of the displacement threshold may also be a factor. A low energy exponent would be expected when the first displacement is created in a low threshold direction and the second in some higher threshold direction. Such arguments are in qualitative agreement with the displacement damage functions for copper derived by Merkle et al. [28].

Between 0.5 and 20 keV, a power-law exponent of 0.795 is observed. Subcascade formation begins to have a significant influence on the defect formation for cascade energies above 10 keV. A power-law exponent of 1.12 was obtained for simulations between 20 and 50 keV. Although only a relatively small range of energies could

be used to obtain the exponent of 1.12, there are two reasons for believing that the slope change at 20 keV is significant. First, the phenomenon of subcascade formation offers a physical basis for the change. The second reason is statistical; standard errors of the mean values obtained at 10, 20, 30, 40, and 50 keV are quite small. One possible explanation for this higher than linear behavior is the relatively low defect density regions that connect the compact subcasades as shown in Fig. 2. Such regions could exhibit higher defect survival efficiencies because their defect density is similar to relatively low energy cascades, and their contribution could slightly raise the average number of stable displacements.

When the number of surviving defects is divided by the predictions of the NRT model, the effect of subcascade formation is seen in the nearly asymptotic value of this ratio obtained at high energies. For simulations at 100 K, a minimum MD/NRT ratio of 0.301 is found at 20 keV. This ratio slightly increases at higher energies, consistent with the high energy power-law exponent of 1.12 just mentioned. Extrapolation of this ratio to higher energies is somewhat uncertain. Observations of how the cascade/subcascade morphology changes between 10 and
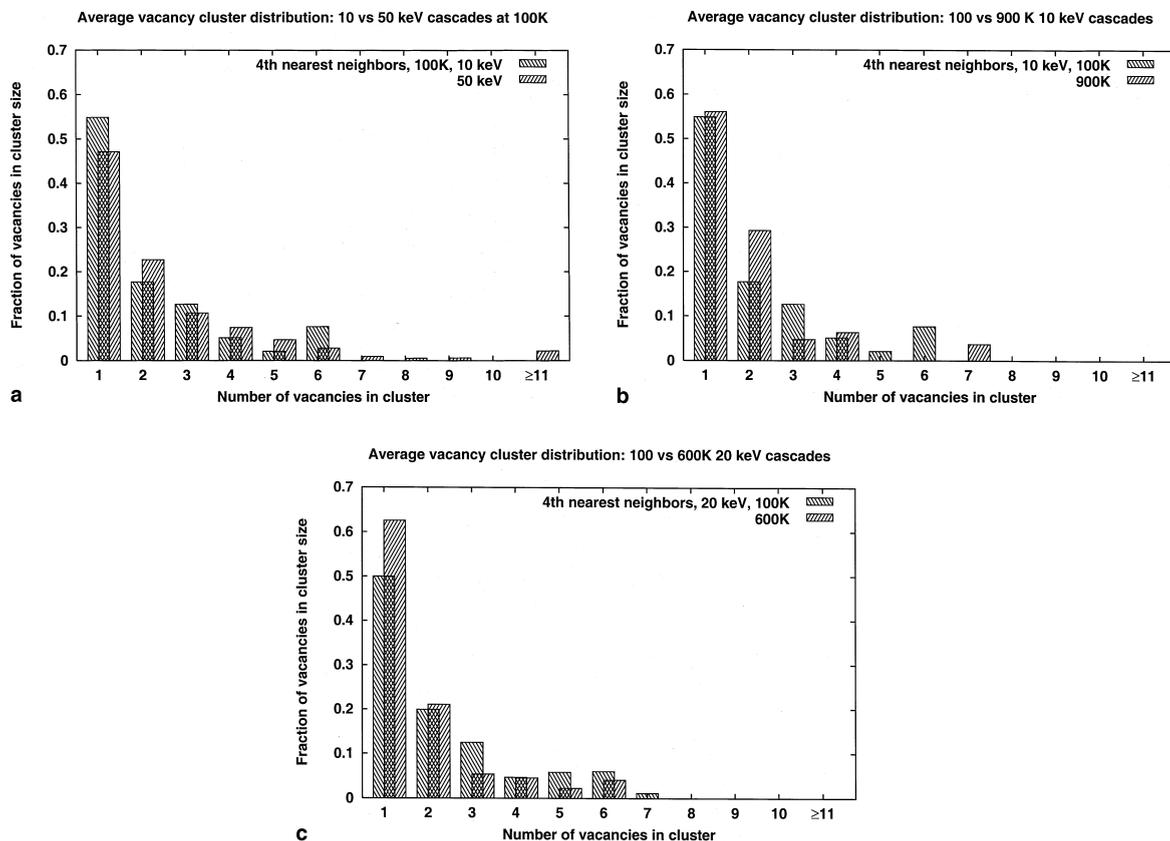

Fig. 9. Fractional size distributions of loosely coupled vacancy clusters (all within 4-nn) formed directly within the cascade, comparison of: (a) 10 and 50 keV cascades at 100 K; (b) 10 keV cascades at 100 and 900 K; (c) 20 keV cascades at 100 and 600 K.

50 keV, and the degree of subcascade formation observed at 50 keV, suggests that higher-energy events should not be qualitatively different. This would imply that the energy dependence should fall to 1.0. However, this conclusion should be verified by at least a limited number of very high energy simulations. In addition, further work is required to confirm that the behavior which is now well documented in 100 K simulations persists at higher irradiation temperatures; some of this work is currently underway.

The effect of subcascade formation is also manifest in the fraction of the defects that form in-cascade clusters. Nearly 60% of the stable, surviving interstitials ($\sim$20% of NRT) formed by high energy cascades are found in such clusters for all cascade energies above 1 keV. The largest such cluster observed contained 33 interstitials. Much less in-cascade vacancy cluster formation is observed. Only about 10% of the stable vacancies ($\sim$3% of NRT) are clustered if the criterion for defining clusters is vacancies in nearest-neighbor locations. However, analysis of the spatial distribution of vacancies suggests that even the quenched-in cascade vacancies may be correlated out to the 4-nn distance. As confirmed by MC cascade annealing studies, such a collection of vacancies can be considered a nascent vacancy cluster that will coalesce when the vacancies have had time to make a few jumps. Accounting for vacancies out to the 4-nn, the clustering fraction is nearly 50% of the total or 15% of NRT. The vacancy clustering fraction also approaches an apparent asymptotic value at high energies. The effect of irradiation temperature on the in-cascade clustering fractions increases as the cascade energy increases.

The size distribution of both vacancy and interstitial clusters shifts to larger sizes as the cascade energy increases. The nature of the temperature effect depends on the defect type. Increasing temperature leads to a further increase in number of large interstitial clusters, but a decrease in the number of large vacancy clusters. As with the total in-cascade clustering fractions, the effect of temperature on the size distribution increases at higher cascade energies. Because of low homogeneous nucleation rates for extended defect production, in-cascade clustering may play a significant role in defect nucleation in irradiated materials, thereby promoting microstructural evolution and concomitant mechanical property changes. In addition, the formation of larger clusters at higher cascade energies could lead to a greater effect of neutron or PKA energy spectrum than is predicted simply on the basis of total defect survival or the total clustering fraction [20].

Acknowledgements

References

[1] R.S. Averback, T. Diaz de la Rubia, R. Benedek, Nucl. Instrum. and Meth. B 33 (1988) 693.

[2] A.J.E. Foreman, W.J. Phythian, C.A. English, Philos. Mag. A 66 (1992) 571.

[3] A.F. Calder, D.J. Bacon, J. Nucl. Mater. 207 (1993) 25.

[4] D.J. Bacon, T. Diaz de la Rubia, J. Nucl. Mater. 216 (1994) 275.

[5] W.J. Phythian, R.E. Stoller, A.J.E. Foreman, A.F. Calder, D.J. Bacon, J. Nucl. Mater. 223 (1995) 245.

[6] R.E. Stoller, in: I.M. Robertson, L.E. Rehn, S.J. Zinkle, W.J. Phythian (Eds.), Proceedings of Symposium on Microstructure of Irradiated Materials, vol. 373, Materials Research Society, Warrendale, PA, 1995, p. 21.

[7] D.J. Bacon, A.F. Calder, F. Gao, V.G. Kapinos, S.J. Wooding, Nucl. Instrum. and Meth. B 102 (1995) 37.

[8] R.E. Stoller, J. Nucl. Mater. 233–237 (1996) 999.

[9] R.E. Stoller, JOM (formerly J. Met.) 48 (1996) 23.

[10] R.E. Stoller, G.R. Odette, B.D. Wirth, J. Nucl. Mater. 251 (1997) 49.

[11] M.J. Norgett, M.T. Robinson, I.M. Torrens, Nucl. Eng. Des. 33 (1975) 50.

[12] ASTM E521, Standard Practice for Neutron Radiation Damage Simulation by Charged-Particle Irradiation, Annual Book of ASTM Standards, vol. 12.02, American Society of Testing and Materials, West Conshohocken, PA.

[13] Yu.N. Osetsky, A. Serra, V. Priego, in: Y. Mishin, G. Vogl, N. Cowern, R. Catlow, D. Farkas (Eds.), Proceedings of Symposium on Diffusion Mechanisms in Crystalline Materials, vol. 527, Materials Research Society, Pittsburgh, PA, 1999, p. 59.

[14] M.W. Finnis, MOLDY6 – A molecular dynamics program for simulation of pure metals, AERE R-13182, AEA Harwell Laboratory, UK (1988).

[15] M.W. Finnis, J.E. Sinclair, Philos. Mag. A 50 (1984) 45.

[16] M.W. Finnis, J.E. Sinclair, Erratum, Philos. Mag. A 53 (1986) 161.

[17] F. Gao, D.J. Bacon, P.E.J. Flewitt, T.A. Lewis, J. Nucl. Mater. 249 (1997) 77.

[18] A. Stuart, J.K. Ord, Kendall's Advanced Theory of Statistics, vol. 1, Griffin, London, 1987.

[19] Manual on Presentation of Data and Chart Control Analysis, sixth edition, American Society for Testing and Materials, West Conshohocken, PA, 1992.

[20] R.E. Stoller, L.R. Greenwood, in: V.V. Butalov, T. Diaz de la Rubia, P. Phillips, E. Kaxiras, N. Ghoniem, (Eds.), Proceedings of Symposium on Multiscale Modeling of Materials, vol. 527, Materials Research Society, Pittsburg, PA, 1999, p. 203.

[21] D.J. Bacon, A.F. Calder, J.M. Harder, S.J. Wooding, J. Nucl. Mater. 205 (1993) 52.

[22] P. Jung, Phys. Rev. B 23 (1981) 664.

[23] G. Wallner, M.S. Anand, L.R. Greenwood, M.A. Kirk, W. Mansel, W. Waschkowski, J. Nucl. Mater. 152 (1988) 146.

[24] B.D. Wirth, PhD dissertation, University of California, Santa Barbara, 1998.

[25] S. Sato, A. Kohyama, N. Igata, Appl. Surf. Sci. 76&77 (1994) 285.

[26] B.D. Wirth, G.R. Odette, in: V.V. Butalov, T. Diaz de la Rubia, P. Phillips, E. Kaxiras, N. Ghoniem (Eds.), Proceedings of Symposium on Multiscale Modeling of Materials, vol. 527, Materials Research Society, Pittsburgh, PA, 1999, p. 211.

[27] M. Valo, R. Krause, K. Saarinen, P. Hautojarvi, J.R. Hawthorne, in: R.E. Stoller, A.S. Kumar, D.S. Gelles (Eds.), Effects of Radiation on Materials, ASTM STP 1125, American Society for Testing and Materials, West Conshohocken, PA, 1992, p. 172.

[28] K.L. Merkle, W.E. King, A.C. Bailey, K. Haga, M. Meshii, J. Nucl. Mater. 117 (1983) 4.